

# Infrared Detector Development Programs for the VLT Instruments at the European Southern Observatory

G. Finger, P. Biereichel, H. Mehrgan, M. Meyer, A. F. M. Moorwood, G. Nicolini and J. Stegmeier

European Southern Observatory  
Karl Schwarzschild Str. 2, 85748 Garching b. München, Germany.

## ABSTRACT

Instrument platforms like the VLT represent a new challenge to infrared focal plane technology. Since the large telescope diameter and the improved image quality provided by adaptive optics reduce the pixel scale, larger array formats are needed. To meet this challenge ESO is participating in development programmes for both InSb and HgCdTe large format arrays. To cover the spectral region of 1 to 5 micron ESO has funded a foundry run at SBRC to produce 1024x1024 InSb arrays which will be installed in ISAAC, the Infrared Spectrometer and Array Camera built for the VLT. Since the delivery of the 1Kx1K InSb array is delayed, test results obtained with a 256x256 InSb array and the application of off chip cryogenic amplifiers to InSb detectors will be discussed.

Results obtained with a  $\lambda_c=2.5\mu\text{m}$  Rockwell 1024x1024 HgCdTe array will be presented where an off chip cryogenic operational amplifier was used yielding a rms read noise of 3 electrons. Sensitivity profiles of individual pixels have been measured with a single mode IR fiber. Limitations of PACE 1 technology such as persistence will be discussed. First results with the 1Kx1K array, which was installed in SOFI, an infrared focal reducer providing 1-2.5 micron imaging and long slit grism spectroscopy at the NTT telescope, will be presented. Advanced techniques of real time image sharpening will also be included. An outlook to the development of  $\lambda_c=2.5\mu\text{m}$  2048x2048 HgCdTe array formats will be given. The concept of NIRMOS, a multi object spectrograph for the VLT telescope, is based on the availability of 2Kx2K HgCdTe arrays.

**Keywords:** infrared detector, infrared array, InSb, MCT, HgCdTe, megapixel, 1024x1024, HAWAII, ALADDIN

## 1. Introduction

During the past decade IR array formats have grown exponentially and have surpassed the megapixel threshold. In parallel to the increased array format the readout noise has been reduced by more than one order of magnitude. This has largely expanded the scope for astronomical observations in the infrared.

Two main projects of megapixel arrays are under development. For the wavelength range of 1 - 5  $\mu\text{m}$  the ALADDIN project, Advanced Large Area Detector Development in InSb, is an effort of the Santa Barbara Research Center, the National Optical Astronomy Observatory and the US Naval Observatory to develop a 1024x1024 InSb array [2], [3]. ESO has placed a contract with SBRC to produce six sensor chip assemblies on a best effort basis. In order to handle the preprocessing of a continuous data rate of 40 megabytes/sec which is generated by 32 parallel video output channels of the Aladdin array, we had to develop a completely new data acquisition system called IRACE. This system heavily relies on parallel processing and is described elsewhere in these proceedings [1].

For the spectral range of 1 - 2.5  $\mu\text{m}$  the HAWAII (HgCdTe Astronomical Wide Area Infrared Imager) array, a 1024x1024 HgCdTe array having a cutoff wavelength of  $\lambda_c=2.5\mu\text{m}$  was developed by Rockwell International Science Center in collaboration with the University of Hawaii [4], [5]. This device is now widely used for ground based astronomical applications. ESO has tested the astronomical performance of this array during the commissioning run of SOFI at the NTT telescope.

The first infrared instrument which will be installed at the VLT is the Infrared Spectrometer and Array Camera

ISAAC. It has two separate cameras optimized for the 1-2.5  $\mu\text{m}$  and 2 to 5  $\mu\text{m}$  ranges. The short wavelength camera is equipped with the Rockwell 1Kx1K HgCdTe array, the long wavelength camera with the SBRC 256x256 or 1024x1024 InSb array. By this separation into two wavelength channels the photon energy is better matched to the bandgap of the infrared detector material. This relieves the requirements of optical baffling and helps to achieve the low darkcurrent needed for high resolution spectroscopy in the non thermal infrared.

To satisfy the need of even larger array formats for multiobject spectroscopy, ESO is participating in funding the development of a 2Kx2K MCT array which will be based on the 1Kx1K PACE1 technology and will produce first science grade arrays within 2 years

## 2.InSb arrays

The optical design of the long wavelength arm of ISAAC can accept both SBRC 256x256 or 1024x1024 pixel InSb arrays. Since 1024x1024 arrays are on order but not delivered yet, we continued the performance evaluation with SBRC 256x256 InSb arrays. Previous test results have been discussed elsewhere [2] , [6] . We use a low doped array which can be reversely biased up to 1.5 V resulting in a storage capacity of  $4.5 \cdot 10^5$  electrons. The quantum efficiency is 0.99 in L, 0.94 in K and 1.16 in the H and J band. In J the photon energy is 4.2 times the bandgap energy. Hence, an internal gain mechanism similar to effects well known in silicon CCD's must be assumed in order to explain the excess quantum efficiency which is larger than uncertainties of the calibration. This effect has also been observed at SBRC.

### 2.1.Darkcurrent

The temperature dependence of the dark current has been re-examined in a new cryogenic setup. Since a temperature sensor mounted on the cold braid close to the detector did not represent the detector temperature because of poor thermal contacts, the temperature was read from the silicon diode bonded on the LCC package of the array. Due to the high thermal impedance of the cooling chain, which connects the detector to the second stage of the closed cycle cooler, the cooling power at the detector is limited to a few mW at temperatures below 40 K. As a consequence additional thermal isolation of the detector from the cryogenic detector board by a 10 cm long flexible manganin cable was necessary. With these modifications subelectron darkcurrents could be achieved as demonstrated in figure 1. The logarithm of the darkcurrent is plotted versus the inverse temperature. The temperature dependence of the darkcurrent is indicative for a surface current g-r mechanism which is proportional to  $\exp(-E_g/mKT)$  with  $m=2$ . A fit to experimental data yields  $m=1.94$ . Sampling a 10 hour integration ramp, the darkcurrent measured at 36.12 K is 0.073 e/sec.

### 2.2.Readout Noise

By applying 64 multiple nondestructive readouts on a 12.7 sec integration ramp we obtained a readout noise of 23 electrons rms. The noise was calculated from a series of identical dark exposures. We also tried to use cryogenic operational amplifiers next to the detector. In our setup the power dissipation of the cryogenic amplifiers raised their temperature to 114 K. As a consequence, the detector signal generated by the thermal radiation of the amplifiers was  $\sim 200$  e/sec. This means, that better cooling of the amplifiers and optical screening of the detector is needed.

### 2.3.Development of large format 1024x1024 InSb arrays (Aladdin)

ESO has an ongoing contract with SBRC to produce six 1024x1024 InSb arrays on a best effort basis. Up to this date we have only read out the Aladdin multiplexer using IRACE, the 32 channel high speed data acquisition system built at ESO. The delivery of the first sensor chip assemblies has been delayed due to problems with hybridized arrays, which may display Photon Emitting Defects (PED's). These areas of excessive glow are caused by a current flowing between the detector and the multiplexer. They only show up after hybridization and are not intrinsic to the multiplexer. A technique has been developed at SBRC to remove these PED's by a photolithographic etching technique

minimizing the loss of pixels (2x2). We expect the delivery of the first ALADDIN arrays next month.

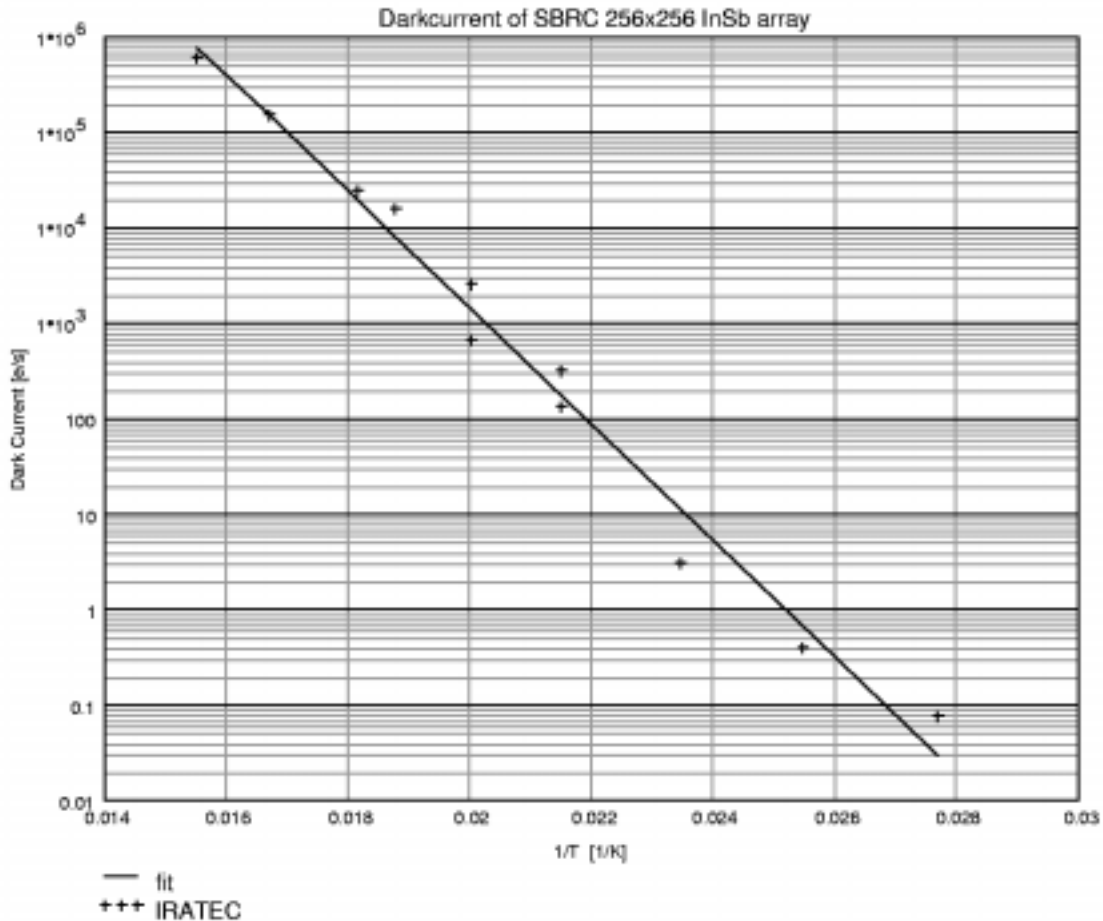


Figure 1 : Dark current versus temperature for the low doped SBRC 256x256 InSb array indicative for a surface current g-r mechanism. Darkcurrent  $\exp(-E_g/mKT)$  with  $m=1.94$ . Darkcurrent is 262 electrons/hour at temperature of 36 K

### 3.HgCdTe arrays

The performance of the Rockwell 1024x1024 HgCdTe array has been described in a previous paper [8] . The quantum efficiency is 0.49 in J, 0.65 in H and 0.64 in K. Darkcurrent measurements have been repeated with improved heat sinking of the detector. At temperatures of 66 K and 78 K the integration ramp was sampled for 3 hours. The accuracy of the derived slope of the integration ramp is dominated by electrical drifts of the signal, so that only an upper limit for the darkcurrent can be given. The darkcurrent is < 30 electrons/hour at a temperature of 78 K.

#### 3.1.Gain

All detector parameters depend on the accurate determination of the gain of the acquisition chain. The gain was calibrated by measuring the shot noise as a function of detector signal at high photon flux levels when the photon shot noise dominates the detector readout noise. The variance of the detector signal is plotted versus the detector signal. The inverse slope of the regressional line fitted to the measured data points yields the pixel transfer function in units of electrons/ADU. The gain of the amplifier in front of the ADC is under computer control. By this method the gain of 5.89 electrons/ADU for the low amplifier gain and 1.29 e/ADU for the high amplifier gain has been determined.

The described calibration scheme is completely independent of any system gain. The voltage gain of the two-stage on-chip source follower was measured by keeping the reset switch permanently closed during the detector readout, while changing the external detector bias voltage and observing the dc shift of the video output. A voltage gain of 0.82 has been determined at a temperature of 65 K for the unit cell source follower. From the measured pixel transfer function of 5.89 e/ADU and the measured voltage gain of the complete signal chain the capacity of the integrating node can be retrieved. It is 41 fF at an external bias voltage of -1 V. The value quoted by the manufacturer is 20 fF.

### 3.2. Readout noise

In order to achieve optimum noise performance in the noisy environment of an infrared instrument with closed cycle coolers and cryogenic stepper motors running close to the low video signals of the detector we have tried different readout schemes for the Hawaii 1024x1024 MCT array. On the readout multiplexer an output source follower is implemented for each quadrant to which the internal video signal bus is connected. This source follower increases the drive capability of the video signal. The user also has direct access to the internal signal bus. Leaving the bias power of the constant-current generator for the horizontal bus as well as drain and source of the output source follower floating, the internal bus can be connected to +5 volt by an external 200K $\Omega$  load resistor. The internal bus is directly connected to the input of an external operational amplifier which is next to the detector and has to operate at cryogenic temperatures. A linear CMOS operational amplifier was selected (Texas Instruments LinCMOS TLC274). For frequencies above 30 Kz it has an equivalent input noise voltage of  $15\text{nV}/\sqrt{\text{Hz}}$  at room temperature and contributes ~ 3 electrons rms to the readout noise of a double correlated clamp. The detector is read out by the home built Infrared Detector High Speed Array Control and Processing Electronics IRACE which is described elsewhere in these proceedings [1]. In the IRACE setup for the Hawaii array the gain of the instrumentation amplifiers in front of the ADC's can be switched from 24 $\mu\text{V}/\text{ADU}$  to 5.3  $\mu\text{V}/\text{ADU}$ . We selected a rise time of 2  $\mu\text{sec}$  for the video signal when reading the array at frame rates of 1 Hz.

Noise measurements under low background conditions were performed in SOFI in the spectroscopy mode. A cold mask with an array of 5x5 pinholes of 100  $\mu\text{m}$  diameter was put in the telescope focus which produces an array of spectra on the detector. To reduce the effective readout noise, multiple nondestructive sampling was applied. After the array is reset it is read out nondestructively at a frame rate of 1 Hz. Each frame samples the integration ramp and improves the accuracy of the regressional fit of the integration ramp. The fit is performed in real time during the ongoing integration. In principle, the readout noise can be reduced to negligible amounts and is reduced by a factor of  $\sqrt{6(n-1)/(n(n+1))}$  with respect to simple double correlated sampling, n being the number of nondestructive readouts. The readout noise shown in Figure 2 was computed for each pixel from a sequence of frames taken under identical conditions. The data points show the peak of the noise histogram of the corresponding noise image. It contains all drifts of the signal chain and illumination levels and has to be carried out under extremely stable conditions.

The expected noise reduction by multiple sampling is shown by the curves decreasing with stare time. The curve increasing with time is the shot noise associated with the darkcurrent. The measured data points well match the combined noise (read & shot noise). The best readout noise of 6.3 electrons rms is achieved at stare times of 1 minute with 64 nondestructive readouts and becomes limited by the quantization noise of the ADC, since the gain is 5.89 electrons/ADU. The same measurement was repeated with higher amplifier gain reading out a 256x256 window every 108 msec. Due to the smaller number of pixels per frame more frames can be read for a given stare time. As a result the read noise can be brought down to values as low as 3 electrons rms with 64 nondestructive readouts performed during stare times of 7.16 seconds. Figure 3 shows the corresponding noise hisyogram.

### 3.3. Sensitivity profile of single pixel

Many instrument designs rely on the ability to concentrate at least 80% of the light of a point source on one pixel. This results in complex optical designs and raises the question whether all signal is generated in one single pixel, if the spot size of the point source imaged onto this pixel is small compared to the pixel size. To investigate this problem we measured the sensitivity profile of a single pixel. This profile is required for modeling the overall MTF of the instrument including optics and detector. It helps the instrument designer to define the required optical quality. If the sensitivity profile of a single detector pixel is accurately known the mechanisms which reduce the quantum efficiency

of the detector can be separated. The slope of the sensitivity profile yields the diffusion length of the minority carriers of the detector material. For spot scans of single pixels fast optics is needed to produce an infrared spot which is small compared to the pixel size of  $18.5 \mu\text{m}$ . Since the FWHM of the airy disk is  $\sim \lambda f^\#$ , the focal ratio 3.09 of the ISAAC objective used has a diffraction limited FWHM of  $6.7 \mu\text{m}$  at the wavelength  $\lambda = 2.17 \mu\text{m}$ .

In these tests one end of an infrared fiber having a core diameter of  $6.5 \mu\text{m}$  was illuminated by a blackbody, the other fiber end was imaged by a star simulator into the telescope focus and re-imaged by the ISAAC optics onto a single detector pixel. The star simulator was mounted on a 3-axis translator stage and moved to generate a grid of spot positions on the detector separated by  $2.16 \mu\text{m}$ .

Figure 4 shows a perspective plot of the spot scan. The response of three adjacent pixels in a row is plotted versus spot position. The energy contained in the next neighbors of the pixel on which the spot is centered is 15% for the column (slow shift register) direction and 6% for the row (slow shift register) direction. The energy concentrated on the central pixel is 58% of the total energy. The spot scan is probably a convolution of the optical spot profile and the detector response. The quoted values are worst case limits. The variation of the total integrated intensity for different spot positions is 7.5% rms and 36% peak to peak and slightly shows the row structure of the array.

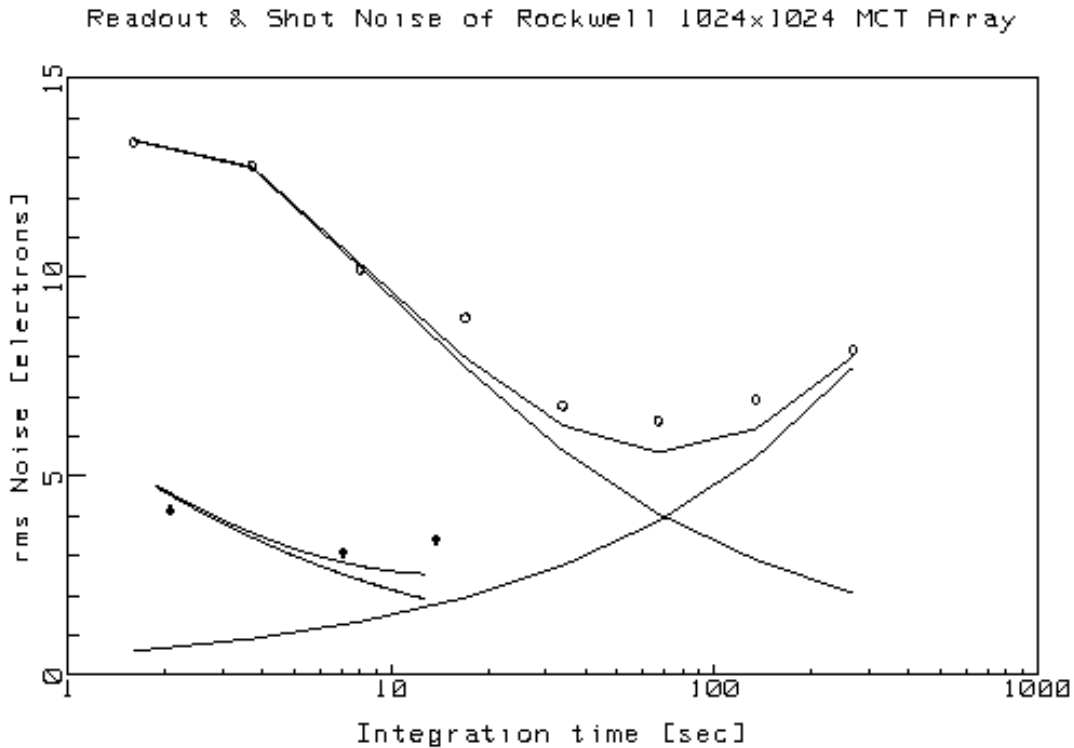


Figure 2 : Readout noise as function of integration time for continuous multiple nondestructive sampling. Frame rate of nondestructive readout is 1 Hz for full frame (upper curves and data points represented by circles) and 9.2 Hz for windowed readout (lower curves and data points represented by stars). Decreasing curves: expected noise reduction by multiple sampling. Increasing curve: Shot noise of darkcurrent. Measured data points match combined noise (read & shot noise).

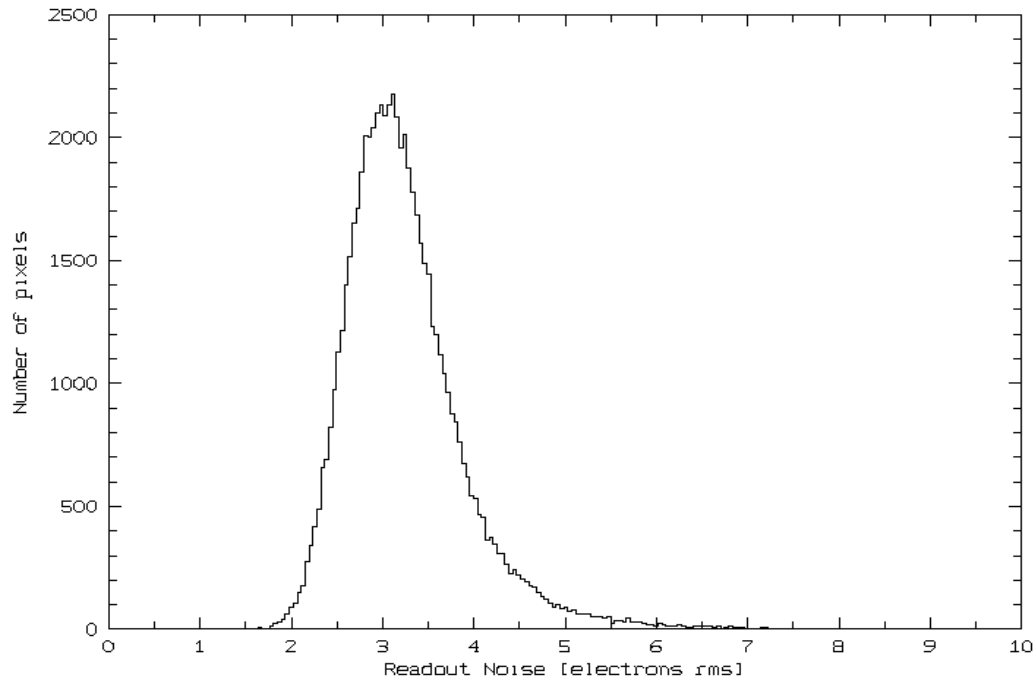


Figure 3 : Histogram of readout noise for a 256x256 pixel windowed readout. Stare time 7.16 seconds with 64 non-destructive samples per stare time.

If the fastest ISAAC objective ( $f/1.7$ ) will be installed the spot quality can be improved. Yet, this is difficult since the alignment has to be checked with pixels much larger than the optical spot diameter. The sensitivity profile of the detector is mainly determined by the diffusion length of the minority carriers. The location where the photon generates the signal charge is dependent on the absorption coefficient of the IR active material. The electron hole pair has to diffuse to the pn junction where it is separated by the electric field of the depletion region. Since the width of the depletion region depends on the bias voltage, the sensitivity profile may also depend on the bias voltage.

### 3.4.Shadowing effects:

The first effect can be seen at low light levels in the center of raw unsubtracted images as a bright horizontal stripe at the quadrant borders. It is caused by the readout topology of the array. Two quadrants have the first rows being read out in the center of the array. The stripe of increased intensity at the beginning of the readout is also unstable and a region of increased noise. We tried different clocking schemes to reduce the effect. Best results were obtained by clocking the fast shift register 64 times without application of the frame start pulse prior to each readout.

The second effect is observed with very bright sources which increase the signal of all pixels lying on the same row. The rows of the other three quadrants of the array being read out at the same time exhibit the same intensity increase. It is not understood why also those pixels of the row which are read out earlier than the bright point source show the same intensity increase. This effect is particularly strong, when a brightly illuminated slit is oriented parallel to the rows. The effect depends on the integrated intensity along the row. This effect has also been observed with NICMOS arrays.

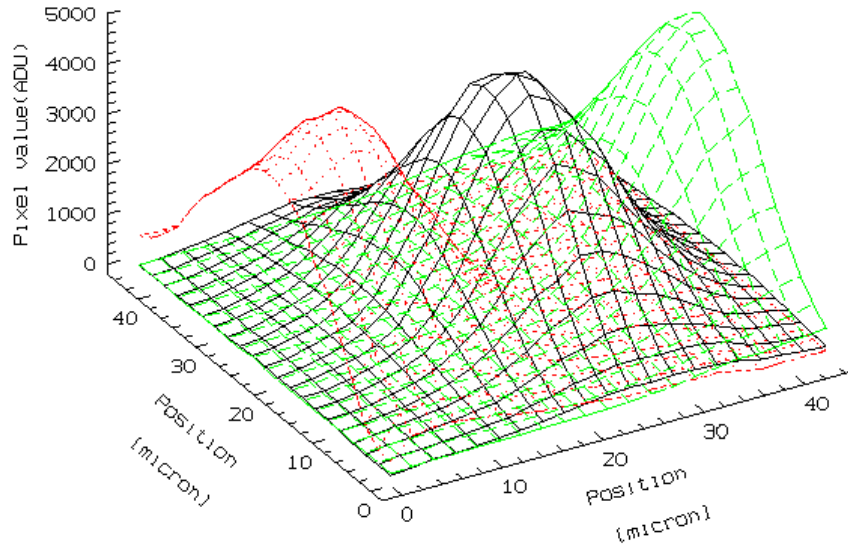


Figure 4 : Sensitivity profile of pixels on 1024x1024 HgCdTe array. Fiber position grid has 21x21 positions with step size of 2.16  $\mu\text{m}$  at detector. Mesh with solid lines shows response of central pixel. Mesh with dashed lines shows response of 2 adjacent pixels.

### 3.5.Persistence

If the detector field of view contains a bright radiation source the subsequent dark exposures exhibit residual excess dark current of those pixels onto which the bright source had been imaged in the previous exposure. This persistence effect of the HAWAII device is strongly reduced in comparison to the NICMOS 3 array, the predecessor of the HAWAII detector [6]. To reduce the persistence we routinely apply 64 full frame resets prior to each double or multiple correlated readout. The persistence effect could not be completely eliminated in the HAWAII detector as demonstrated by a series of specific tests.

In these tests an infrared fiber was used with a core diameter of 6.5  $\mu\text{m}$ . One fiber end was looking into a blackbody at a temperature of 400 Celsius. The aperture of the blackbody can be opened and closed by a shutter. The other fiber end was imaged by a star simulator into the telescope focus and re-imaged by the SOFI optics onto a single detector pixel. The broad band J filter was used. The focal ratio  $f^\#$  of the objective was 3.76. When the shutter of the blackbody is open the flux on one pixel is  $510^6$  photons/sec. After the source was switched off, a series of 10 second dark exposures was taken. The decay of the integrated intensity of the residual images in the 10 second dark exposures is shown in figure 5. It is exponential and can be described by two time constants  $\tau_{c1,2}$ . During the first minute  $\tau_{c1}$  is 11 sec. After 1 minute the decay of the residual image slows down and is described by  $\tau_{c2}$  of 48 seconds. The persistence was measured at detector temperatures of 60K, 65K and 80K, but it does not show any effect on temperature. Since the persistence effect cannot be suppressed completely, care should be taken that for low background observations prior exposure to bright sources is avoided. It takes up to four minutes until the latent image has decayed.

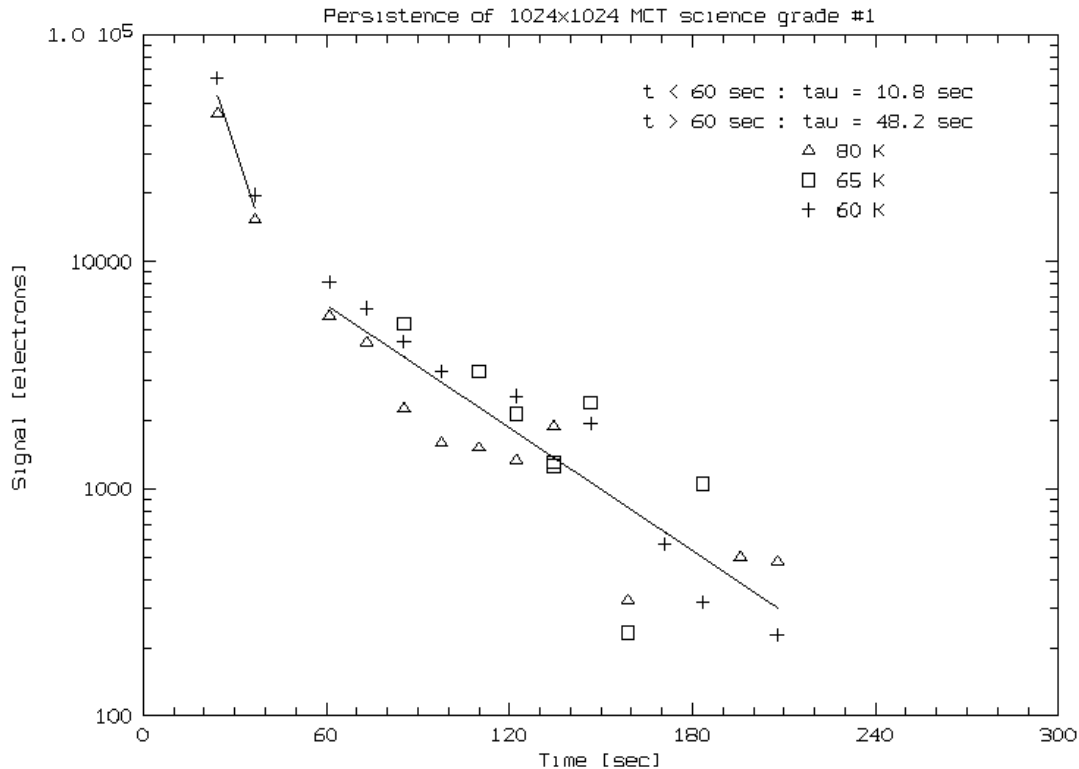


Figure 5 : Persistence effect for different temperatures: Total integrated intensity of latent point source images versus time after switching off point source which exposes the detector to  $510^6$  photons/sec. Integration time of images is 10 sec. Exponential time constant  $\tau=48$  sec for  $t>60$  sec.

#### 4.Astronomical Performance of Rockwell 1024x1024 MCT

##### 4.1.The 1-2.5 $\mu\text{m}$ imager / spectrometer SOFI

First astronomical results with the 1Kx1K array, which was installed in SOFI, ESO's new imager / spectrometer, were obtained at the 3.5 meter New Technology Telescope NTT on LaSilla in December 1997 [7]. SOFI is an infrared focal reducer providing 1-2.5 $\mu\text{m}$  micron imaging, polarimetry and long slit grism spectroscopy. The layout of the instrument is shown in figure 6. The first wheel behind the entrance window is cooled to liquid nitrogen temperature like all the rest of the optics. It is equipped with field masks, slits for spectroscopy, and a special mask for polarimetry using a Wollaston prism. The large 12 cm diameter, diamond turned BaF<sub>2</sub> collimator lens produces an image of the telescope pupil on a 25 mm diameter Lyot stop. Two filter wheels and the grism wheel, which also carries the Wollaston prism and a focal elongator, are placed in the parallel beam. The currently installed grisms are directly ruled on KRS5 and yield a spectral resolution of  $R \sim 300-1000$  depending on which of the 2, 1 or 0.6" wide slits is selected. The last wheel carries three objectives forming the images of varying pixel scales on the detector. The largest field is 5'x5' corresponding to a pixel scale of 0.29"/pixel. Further scales are 0.26"/pixel, 0.14"/pixel or 0.072"/pixel in combination with the focal elongator. It is planned to add a cross dispersed high resolution mode which will extend the spectral resolution to  $R \sim 3500$  by use of etched Si wafer gratings bonded to Si prisms. The optics is cooled to 80K and the detector is stabilized at a temperature of 60 K by a closed cycle cooler. The functions are driven by 5 phase cryogenic stepper motors.

The performance assessed during the first test in December 1997 is summarized in Table 1. The point source detection limits were measured for a signal to noise ratio of  $s/n = 5$  obtained in one hour in a 1.5" diameter aperture under normal seeing conditions of 0.75". The sky brightness in units of magnitude per square arcsec is also given. Since

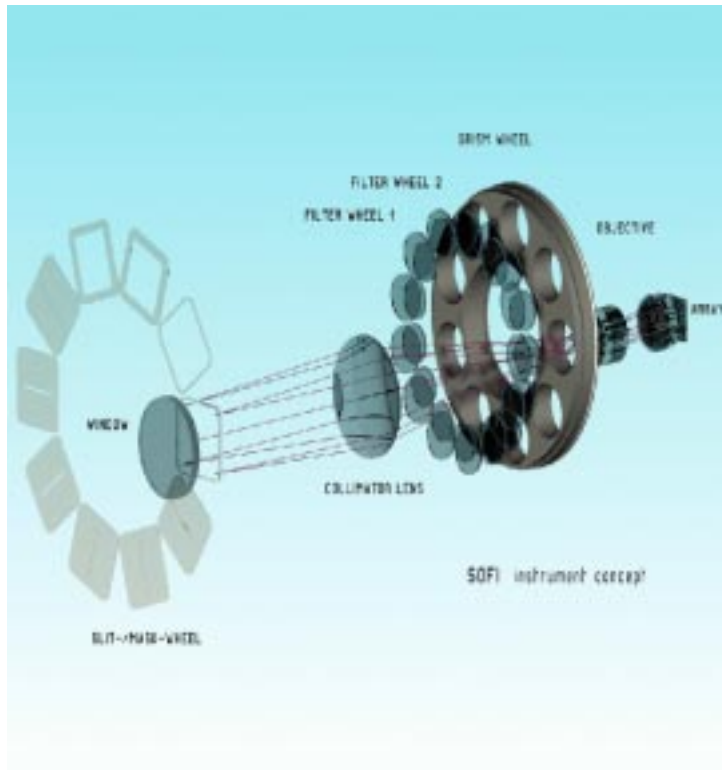


Figure 6 Optical layout of SOFI comprising entrance window, slit-/mask wheel, BaF<sub>2</sub> collimator lens, 2 filter wheels, grism wheel and objective wheel. See text.

SOFI is installed at the Nasmyth platform of the NTT telescope which is not optimized for infrared, the sky brightness of 13th magnitude/square arcsec in the thermal infrared at K is surprisingly low. The thermal background is also stable and free of temperature gradients.

**Table 1:** Point source detection limits of SOFI for a signal to noise ratio of 5 in 1 hour

	<b>measured detection limit</b>	<b>sky brightness</b>
<b>Filter</b>	<b>magnitude</b>	<b>magnitude/square arcsec</b>
<b>J</b>	<b>22.9</b>	<b>16</b>
<b>H</b>	<b>21.9</b>	<b>14.3</b>
<b>Ks</b>	<b>20.9</b>	<b>13</b>

An example of powerful imaging with SOFI is the true colour image of the tarantula nebula in the Large Magellanic Cloud (30 Doradus) which is shown in figure 8. The image is composed of 3 exposures taken with narrow band filters centered on the Br $\gamma$  atomic hydrogen line at 2.166  $\mu$ m (coded blue), the FeII line at 1.644  $\mu$ m (coded green) and the molecular hydrogen line H<sub>2</sub> 1-0 S(1) at 2.12  $\mu$ m (coded red). The exposure time for each line image was 5 minutes. The colour coding represents the ionization state of the gas with red indicating star forming regions. In the image the boundaries of the detector quadrants can no longer be detected.

The bright star of magnitude 6 north east of the center generates a shadowing effect as discussed in chapter 3.4. This bright point source increases the signal of all pixels lying on the same row (rows are vertical in the image) by  $5 \cdot 10^{-5}$  of the peak intensity of the point source. The row is reflected in all four quadrants read out at the same time. The respective rows exhibit the same intensity increase. The shadowing of the central rows is suppressed effectively and



Figure 7 True colour image of 30 Doradus. Blue:  $\text{Br}\gamma$  atomic hydrogen ( $2.166 \mu\text{m}$ ). Green: FeII ( $1.644 \mu\text{m}$ )  
Red:  $\text{H}_2$  1-0 S(1) ( $2.12 \mu\text{m}$ ). (coded red). Exposure time: 5 minutes in each filter. The scale is  $0.26''/\text{pixel}$  and the field is  $4.5' \times 4.5'$ . North is top east left.

the quadrant borders are not visible.

#### 4.2. Image sharpening by real-time on chip tracking

The excellent noise performance, low dark current and high quantum efficiency achieved with the HAWAII array make it a suitable device as an IR wavefront sensor. Furthermore, at telescope foci without adaptive optics and tip tilt mirrors image sharpening can be achieved by on-chip tracking techniques [9], [10]. In the multiple nondestructive readout mode the difference of two consecutive nondestructive readouts is a short time exposure with an integration time equal to the sampling interval. The advantage of taking short time exposures by this method is the following: For a double correlated readout only one nondestructive readout is required instead of two, since the previous readout can be used for subtraction. Therefore, at least a factor of 2 in bandwidth is gained. Because readouts need not be taken immediately after the reset of the array, the disturbance of the first nondestructive readout by the array reset is avoided.

These short time exposures can be re-centered to compensate for image motion induced by atmospheric turbulence. The time interval between two nondestructive readouts must be at least as long as the readout time of the array. It is the critical parameter for these applications. Since it takes 1 second to read out the whole array and readout times of less than 100 msec are required to achieve substantial improvement of image quality in K band by first order wave-front corrections we decided to confine the tracking algorithm to a window of 256x256 pixels which can be read out in 122 msec.

For SOFI, which is installed at the 3.5 m NTT telescope model calculations predict a gain in Strehl ratio of 4 [8]. Figure 8 shows a three-dimensional plot of a subwindow of cluster NGC2808 observed in K band. The pixel scale of the image is 72 milli arcsec/pixel. On the left side the point sources of the untracked image has a FWHM of 0.53". The tracked image is shown on the right side of figure 8. Tracking of the image reduces the FWHM of the central spike on top of the halo of the seeing disk to 0.21" and improves the Strehl ratio by a factor of 3.3.

### 4.3.MCT 2048x2048 Development

To study the evolution and large scale structure of the universe several hundred thousand galaxies have to be observed. To accomplish this task, the multiobject spectrograph NIRMOS is being built for the VLT covering the wavelength range from 1 to 1.8  $\mu\text{m}$ . This instrument is driving the demand for even larger array formats since it is designed to house four 2Kx2K detectors. For this reason ESO has signed a contract with ROCKWELL to develop a  $\lambda_c$ -2.5  $\mu\text{m}$  2048x2048 HgCdTe array. The first engineering grade array is expected in February 1999, the first science grade array in October 1999.

To minimize the risk and maximize the yield the detector array will be LPE grown material on sapphire substrate, a mature technology which is used for the production of the 1Kx1K HAWAII arrays. The silicon readout multiplexer will consist of 4 electrically independent quadrants. It will be fabricated on the Si wafer by photocomposition of four 1Kx1K quadrants. The array will be mounted on a pin grid array ceramics which can be plugged into a zero insertion force socket. The central pins can be used for heatsinking the detector. The number of video outputs will be programmable between 4 and 32. Since the analog signal bandwidth can be reduced by using all video outputs, we intend to use all 32 outputs. The data acquisition system of NIRMOS must be capable of reading all 128 channels of four 2Kx2K detectors simultaneously. The IRACE architecture is flexible and well suited for this task.

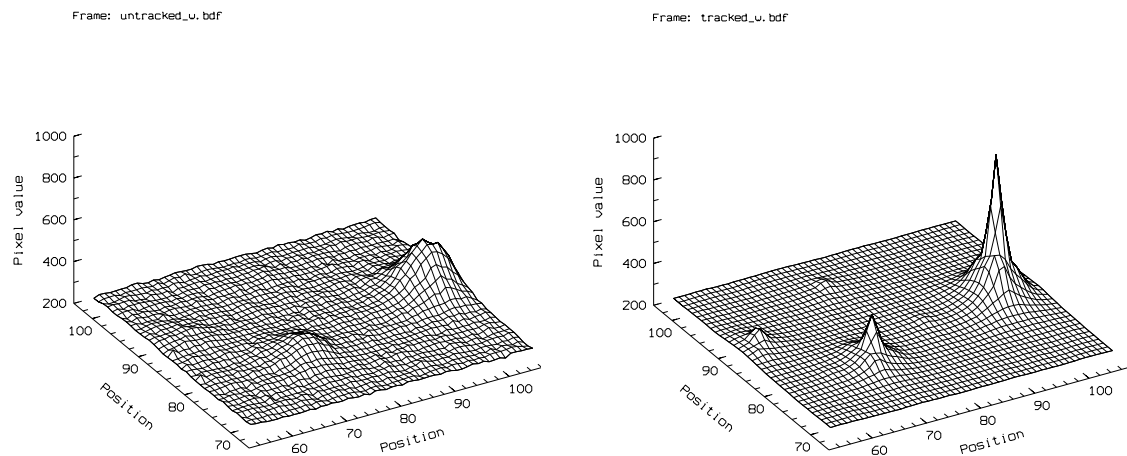


Figure 8 : Real time On-chip tracking: K band image of cluster NGC2808. Pixel scale 72 marcsec/pixel. Left: untracked. FWHM 0.53". Right: tracked. FWHM 0.21" of central spike. Gain in Strehl ratio: 3.3.

## 5.Conclusions

Megapixel IR arrays have become available and have been evaluated in several ground based instruments. The delivery of the 1024x1024 InSb arrays to ESO was delayed due to problems with photon emitting defects of hybridized arrays. Meanwhile, a solution has been found to cure this effect. Subelectron darkcurrent has been measured with a 256x256 InSb array. In view of the low darkcurrent and the high quantum efficiency of InSb it becomes an attractive detector material also for the non-thermal infrared if sufficient shielding of the detector from thermal background radiation can be provided.

Excellent results have been obtained with the 1024x1024 HgCdTe array. Applying multiple sampling techniques a readout noise of 3 e rms could be achieved with external CMOS operational amplifiers bypassing the on chip amplifier. The CMOS amplifiers are next to the detector at cryogenic temperatures. Some of the problems encountered with NICMOS-3 arrays, the predecessor of the HAWAII array, such as amplifier glow and persistence have been substantially reduced. The astronomical performance of a 1024x1024 HgCdTe science grade array has been evaluated with SOFI, ESO's new imager / spectrometer at the NTT telescope. Image sharpening by a simple shift-and-add algorithm performed in real-time improves the Strehl ratio of K-band images on a 3.5 m telescope by a factor of 3.3. The PACE-1 technology of 1Kx1K HgCdTe arrays is being extended to formats of 2Kx2K and will further expand the frontiers of infrared astronomy.

## 6.Acknowledgments

The authors wish to thank J. Cuby and C. Lidman who observed and reduced astronomical data taken during the SOFI commissioning run.

## 7.References

- [1]. M. Meyer, G. Finger, H. Mehrgan, G.Nicolini and J Stegmeier, "The ESO Infrared Detector High Speed Array Control and Processing Electronic IRACE", Proceedings SPIE 3354, 1998.
- [2]A. M. Fowler and J. Heynssens, "Evaluation of the SBRC 256x256 InSb focal plane array and preliminary specification for the 1024x1024InSb focal plane array", Proceedings SPIE 1946, pp. 25-32, 1993.
- [3]A. M. Fowler, I. Gatley, F.J. Vrba, H.D.Ables, A. Hoffman and J. Woolaway, "Aladdin, the 1024x1024 InSb Array: Test Results", Proceedings SPIE 2475, pp. 27-33, 1995.
- [4]L.J. Kozlowski, K. Vural, S.A.Cabelli, C.Y. Chen, D.E. Cooper, G.L Bostrup, D.M. Stephenson, W.L. McLevige, R.B.Bailey, K. Hodapp, D.Hall and W.E. Kleinhans, "2.5  $\mu$ m PACE-I HgCdTe 1024x1024 FPA for Infrared Astronomy", Proceedings SPIE 2268, pp. 353, 1994.
- [5]K.W.Hodapp, J.L.Hora, L.L.Cowie, M.Metzger, E.Irwin, D.Hall, K. Vural, L.J. Kozlowski, S.A.Cabelli, C.Y. Chen, D.E. Cooper, G.L Bostrup, R.B. Bailey, W.E. Kleinhans, "The Hawaii Infrared Arrays: Testing and Astronomical Characterization of Prototype and Science-Grade Devices", to be published in New Astronomy.
- [6]G.Finger, G.Nicolini, M. Meyer, and A.F.M. Moorwood, "High well capacity InSb arrays for the 1 to 5  $\mu$ m wavelength range", Proceedings SPIE 2475, pp. 15-26, 1995.
- [7]A. Moorwood,J.-G. Cuby, and C. Lidman, "Sofi Sees First Light at the NTT", The Messenger 91,pp. 9-13,1998
- [8]G. Finger, P. Biereichel, H. Mehrgan, M. Meyer, A. F. M. Moorwood, G. Nicolini and J. Stegmeier,"Megapixel Infrared Arrays at the European Southern Observatory", Proceedings SPIE 2871, pp 1160-1170,1996.
- [9]G. Finger, P Biereichel, M. Meier and A.F.M. Moorwood, "Image Sharpening by On-Chip Tracking in IRAC2", Proceedings SPIE 1946, pp. 134-145, 1993.

- [10]G. Finger, P Biereichel, A. van Dijsseldonk, M. Meier and A.F.M. Moorwood, "Real Time Image Sharpening without Adaptive Optics by On-Chip Tracking", Proceedings SPIE 2198, pp 763-773, 1994.